RSC Advances

Journal Name

ARTICLE

Gas Separation Membranes Made through Thermal Rearrangement of *ortho*-methoxypolyimides

Bibiana Comesaña-Gándara [a,b,c,d], José G. de la Campa [a,*], Antonio Hernández [b], Hye Jin Jo [d], Young Moo Lee [d,*], Javier de Abajo [a], Angel E. Lozano [a,b,d,*]

Ortho-methoxypolyimides were prepared from 3,3'-dimethoxybenzidine (DMAB) and hexafluoroisopropylidene diphthalic anhydride (6FDA). High molecular weights of the resulting polymers were achieved, and the physical properties of the materials were investigated. The polyimides exhibited excellent thermal properties and film-forming capabilities. Polyimides were treated at high temperatures to promote thermal rearrangement (TR) processes. The final composition of the TR polymers seemed not to correspond to TR-polybenzoxazoles, as was the case when analogous ortho-hydroxypolyimides were exposed to similar thermal treatments. A detailed study was carried out to elucidate the actual mechanism of thermal rearrangement, comparing ortho-hydroxypolyimides, ortho-acetylpolyimides and ortho-methoxypolyimides. Results led to the conclusion that the chemical nature of the final TR polymers attained from ortho-methoxypolyimides is complex since imide, lactam and benzoxazole groups all seem to be present after thermal treatment. Gas permeation properties exhibited by thermally treated ortho-methoxypolyimides compared well with those of other TR-PBOs, showing CO_2 permeability of 540 Barrers.

Introduction

Polymer membranes are widely regarded as an important class of materials, when accompanied with classical separation techniques, for the separation of gases, because membranes offer a more energy-efficient separation process than other techniques [1–5]. In addition, membrane technology is a much more environmentally friendly process with low footprint than, for instance, traditional absorptive technologies. In this regard, some examples of industrial interest can be mentioned: O_2 or N_2 enrichment [6,7], natural gas sweetening [8,9], air drying [10,11], recovering of H_2 from the purge gas created during ammonia synthesis or syngas production [12,13], recovering of toxic, volatile monomers such as vinyl chloride [14], olefin/paraffin separation [15–17], recovering of CO_2 and acid gases from flue gas mixtures [18,19].

For a polymer membrane to be a potential candidate for gas separation, it must show excellent separation properties, which means that it should simultaneously offer high gas permeability and high selectivity.

Gas transport through polymer membranes proceeds by a sorption-diffusion mechanism that involves both diffusion of gas molecules through the polymer material and interactions of the gas and the polymer at the molecular scale. These processes can be defined in terms of the diffusivity coefficient (kinetic component) and a solubility coefficient (thermodynamic component), as depicted in Equation 1:

$$P = D \cdot S \qquad (1)$$

The existence of a trade-off between permeability and selectivity has been clearly observed [20,21]. Because of this, most polymers are balanced so that a high permeability means a poor selectivity and *vice versa*. Significant efforts have been devoted to finding polymer compositions that provide good permeability and selectivity at the same time [22]. Several authors have proposed diverse ways of circumventing the trade-off in order to discover new gas separation materials with enhanced properties [15,22,23].

In this context, a new class of polymeric materials has recently been developed; it offers a suitable approach for making efficient gas separation membranes. Aromatic polyimides (PIs) containing free –OH groups, *ortho*-positioned with respect to the imide ring, have achieved significant attention as they can be converted into polybenzoxazoles (TR-PBOs) by a controlled thermal rearrangement process in the solid state at high temperatures [24]. In this work, CO_2 permeability well over 1000 Barrers were reported for the thermally treated *ortho*-

a. *Institute of Polymer Science and Technology, ICTP-CSIC, Madrid, Spain*
b. *SMAP UA-UVA_CSIC, University of Valladolid, Valladolid, Spain*
c. *IU Cinquima, University of Valladolid, Valladolid, Spain*
d. *Department of Energy Engineering, College of Engineering, Hanyang University, Seoul 133-791, Republic of Korea*
*(A. E. L) Telephone: +34-91-561-88-06 Ext. 320; E-mail. lozano@ictp.csic.es
*(J. G. C) Telephone: +34-91-562-29-00 Ext. 350; E-mail. jcampa@ictp.csic.es
*(Y. M. L) Telephone: +82-2-2220-0525; E-mail. ymlee@hanyang.ac.kr

hydroxypolyimide derived from 2,2'-bis (3-amino-4-hydroxyphenyl)-hexafluoropropane (APAF) and hexafluoroisopropylidene diphtalic anhydride (6FDA). These outstanding results have pushed the membrane community to make additional efforts to optimize the methods and to seek alternative monomers, improving the whole synthesis process and helping to find an attractive combination of low-cost, process feasibility and gas separation performance [25–27]. Fluorinated monomers are expensive, therefore other aromatic monomers, particularly wholly aromatic diamines derived from the biphenylene residue, have been assayed, and promising results have been achieved [28,29]. Additionally, to assure the facile processing of the *ortho*-hydroxypolyimides the use of dianhydride 6FDA seems to be necessary to keep soluble polyimides that can eventually be transformed into membranes by polymer solution casting.

The generally accepted mechanism for the imide-to-polybenzoxazole thermal rearrangement involves the decarboxylation of *ortho*-hydroxypolyimide at high temperatures (well over 350 °C) through the formation of a carboxy-benzoxazole by the elimination of a CO_2 molecule [24,30]. Additionally, other functionalized polyimides have been studied as precursors, particularly polyimides containing *ortho*-ester groups [31]. The use of esters instead of hydroxyl-free groups seems to eventually render PBOs that show slightly higher permeation performance than those prepared from *ortho*-hydroxypolyimides. In addition *ortho*-ester polyimides simultaneously offer better solubility and a lower glass transition temperature. Guo *et al*. have recently reported about the effects of different *ortho*-functional groups on the transformation of polyimide precursors into polybenzoxazoles and on their permeation properties [31]. These authors observed that using *ortho*-esterpolyimides significantly affected the rearrangement process, and that by changing the –OH groups into RCOO- groups enhances permeability due to the increased free volume provided by the larger ester group (when compared to the hydroxyl group).

Based on these precedents, and looking for new routes towards TR-PBO polymers, a study was performed on the preparation and evaluation of TR-PBO materials obtained from *ortho*-methoxy containing polyimides. The thermal rearrangement of *ortho*-methoxy-polyimides to TR-PBOs was recently reported [32], however, a detailed study of the mechanism was not done at that time, nor any investigation on the gas permeation properties. Additionally, polybenzoxazoles have been attained from *ortho*-methoxy aromatic polyamides, mainly by looking for a substantial thermal resistance increase of the precursor polyamides [33]. Other authors used this approach to prepare PBOs with various end-goals [34,35]. However, these precursors with side methoxy groups have not been studied for TR-PBOs in gas separation applications.

In this work, we report on the preparation of soluble *ortho*-methoxy polyimides made from 6FDA dianhydride and 3,3'-dimethoxybenzidine, which is a comparatively low-priced monomer. The conversion of this precursor into TR-PBO at high temperatures was the objective of this study and our

focus consisted of the search of time tratment vs temperature schedule relationships and also on determining the final properties of films fabricated from the precursor. Special attention was given to the possible reactions that occurred alongside the thermal treatment. Results were compared with *ortho*-hydroxy and *ortho*-acetylpolyimides of similar structure and to the permeation properties of the final films in comparison with earlier reported TR-PBOs.

Experimental Section

Materials

Chlorotrimethylsilane (CTMS), pyridine (Py), 4-dimethylaminopyridine (DMAP), o-xylene, acetic anhydride and anhydrous N-methyl-2-pyrrolidinone (NMP) were all provided by Aldrich (Milwaukee, WI, USA) and used as received. Aromatic diamines 3,3´-dihydroxybenzidine (HAB) and 3,3´-dimethoxybenzidine (DMAB) were supplied by TCI Europe (Amsterdam, Holland) and Aldrich, respectively. HAB was dried at 120 °C for 5 h under vacuum and DMAB was sublimed prior to use. 2,2´-bis(3,4-dicarboxyphenyl)hexafluoropropane dianhydride (6FDA) was purchased from Cymit Química (Barcelona, Spain) and sublimed just before use.

Synthesis of Polyimides Derived from 6FDA and HAB

The formation of the hydroxy-containing poly(amic acid) intermediates (*HPAA*) is common during the synthesis of both *PI-OH* and *PI-OAc* structures, with the exception that the solvent employed in the reactions are different. For the chemical imidization process, DMAc was used as a solvent, while NMP was chosen for azeotropic imidization to facilitate water removal. *HPAA* intermediates were prepared using the following general route: 10.0 mmol of HAB diamine and 10 mL of the chosen solvent were added to a round bottomed three-necked flask and stirred at room temperature under a dry nitrogen atmosphere. When the solid had entirely dissolved, the solution was cooled to 0 °C and the required amount of CTMS (1 mol/mol reactive group) was added to the solution, followed by Py (1 mol/mol reactive group) and DMAP (0.1 mol/mol Py). The temperature was subsequently raised to room temperature and maintained for 15 min to ensure the formation of the silylated diamine. After this time, the solution was cooled once again to 0 °C, and a stoichiometric amount of 6FDA (10.0 mmol) was carefully added followed by 10 mL of solvent to rinse the inner flask walls. The reaction mixture was stirred for 15 min and then the temperature was raised to room temperature where it was left overnight to form the *HPAA* intermediates.

To attain the final polyimide with the -OH groups in the *ortho*-position, polyimide designated as *PI-OH*, *o*-xylene (20 mL), as an azeotropic agent, was added to the *HPAA* solution, which was then vigorously stirred and heated for 6 h at 180 °C to promote cycloimidization. During this step, the water released from the ring-closure reaction was separated out as a xylene azeotrope, along with silanol and other siloxane by-products

derived from the use of the silylating agent. Additional *o*-xylene was stripped out from the polymer solution, which was then cooled to room temperature and precipitated in distilled water. The polymer obtained was washed several times with water, then a mixture of water/ethanol (1/1), then pure ethanol, and finally dried in a convection oven at 150 °C for 12 h under vacuum. **PI-OH**: η_{inh} (dL/g) = 1.51. ^{1}H-NMR (DMSO-d_6, 500 MHz): 10.23 (s, 2H, OH), 8.27 (d, 2H), 8.08 (d, 2H), 7.87 (s, 2H), 7.46 (d, 2H), 7.29 (s, 2H), 7.27 (s, 2H). FT-IR (film): v(-OH) at 3401 cm^{-1}, imide v(C=O) at 1785 and 1715 cm^{-1}, imide v(C-N) at 1378 cm^{-1}, imide v(C-N-C) at 1099 cm^{-1}.

In order to obtain -OAc groups in the final polyimide structure, polyimide designated as *PI-OAc*, was obtained from the *HPAA* intermediate that was chemically imidized by adding to the solution a mixture of acetic anhydride (80 mmol, 4 mol/mol reactive group) and Py (80 mmol, 4 mol/mol reactive group). The solution was stirred for 6 h at room temperature and 1 h more at 60 °C to promote complete imidization. The viscous polyimide solution was cooled at room temperature and poured into water where a fibrous precipitate formed that was then repeatedly washed with water and a mixture of water/ethanol (1/1). The precipitate was finally dried in a vacuum oven at 150 °C overnight. **PI-OAc**: η_{inh} (dL/g) = 0.62. ^{1}H-NMR (DMSO-d_6, 500 MHz): 8.22 (d, 2H), 8.00 (d, 2H), 7.86 (s, 2H), 7.80 (m, 2H), 7.68 (d, 2H), 2.16 (s, 6H, CH$_3$). FT-IR (film): imide v(C=O) at 1778 and 1724 cm^{-1}, imide v(C-N) at 1370 cm^{-1}, imide v(C-N-C) at 1096 cm^{-1}.

Synthesis of Polyimides Derived from 6FDA and DMAB *via* Chemical Imidization (PI-OMe)

A three-necked flask was charged with 10 mmol of diamine DMAB and 10 mL of DMAc as a solvent. The mixture was cooled to 0 °C and the required amount of CTMS (20 mmol, 1 mol/mol reactive group) was incorporated, followed by Py (20 mmol, 1 mol) and DMAP (2 mmol, 0.1 mol/mol Py). The solution was allowed to come to room temperature and was then stirred for 15 min to ensure the formation of the silylated diamine. After this, the solution was cooled once again to 0 °C and 6FDA (10.0 mmol) was added followed by 10 mL of DMAc. After 15 minutes of stirring at 0 °C, the solution was allowed to come to room temperature where it was left overnight to form the methoxy-containing poly(amic acid) intermediate designated as *MeOPAA*. Subsequently, the *MeOPAA* intermediate was cyclized into its corresponding polyimide via a chemical imidization process by adding a mixture of acetic anhydride (80 mmol, 4 mol/mol reactive group) and Py (80 mmol, 4 mol/mol reactive group) to the solution. In order to promote complete imidization, the solution was stirred for 6 h at room temperature and 1 h more at 60 °C. The polyimide solution was cooled to room temperature and then poured into water. The precipitate obtained was thoroughly washed with water and ethanol, and then dried at 150 °C for 12 h under vacuum. **PI-OMe**: η_{inh} (dL/g) = 0.59. ^{1}H-NMR (DMSO-d_6, 500 MHz): 8.19 (d, 2H), 8.00 (d, 2H), 7.86 (s, 2H), 7.53 (s, 2H), 7.52 (d, 2H), 7.46 (d, 2H), 3.88 (s, 6H, CH$_3$), FT-IR (film): imide

v(C=O) at 1787 and 1724 cm^{-1}, imide v(C-N) at 1373 cm^{-1}, imide v(C-N-C) at 1099 cm^{-1}.

Formation of Polyimide Films and Subsequent Thermal Treatment

To prepare polyimide films, 10 wt % polyimide solutions in NMP or DMAc (the same solvents used for both polyimide synthesis routes) were filtered through a 3.1 μm glass-fiber syringe filter and cast onto well-leveled glass plates. The films were dried at 60 °C overnight to remove the majority of the solvent and then placed in a vacuum oven. The polyimide films were progressively heated to 250 °C, holding for 1 h at 100 °C, 150 °C, 200 °C and 250 °C under vacuum to remove any residual solvent. Self-supported films were stripped off their glass plates, washed with distilled water, and dried at 130 °C, under vacuum, overnight. Film thicknesses were between 40 and 50 μm and suitable film uniformity was verified by measuring the film thickness standard deviation, which was lower than 5 % for all cases. All polyimide samples were cut into 3 cm x 3 cm defect-free pieces and placed between ceramic plates to avoid film rolling at elevated temperatures. These were placed in a quartz tube furnace under an inert gas. In order to completely remove solvent and to ensure full imide ring closure, all polyimide films were heated at a rate of 5 °C/min to 300 °C and held for 2h for the *PI-OH* film and 1h for the *PI-OAc* and *PI-OMe* films, under 0.3 L min^{-1} nitrogen flow.

The precursor polyimide membranes were converted into TR membranes by a further thermal treatment. To do this, the polyimide membranes were heated to 350 °C, 400 °C and 450 °C at a rate of 5 °C min^{-1}, and maintained there for a desired amount of time (30 min or 1 h) in a high-purity nitrogen atmosphere. This procedure follows a protocol described in literature [28], and in performing such a treatment, all samples were exposed to thermal treatments similar to those previously reported. The cooling protocol consisted of allowing the furnace to reach room temperature at a rate no greater than 10 °C min^{-1}. The thermally treated membranes, obtained from the *PI-OH*, *PI-OAc* and *PI-OMe* precursor polyimides, were designated as TR-OHX, TR-OAcX and TR-OMeX, respectively, where X indicates the final temperature applied to those samples.

Polyimide and Membrane Characterizations

Structural differences between polyimides were confirmed by ^{1}H-NMR spectra obtained from a Varian System 500 nuclear magnetic resonance (NMR) spectrometer operating at 500 MHz. A Perkin Elmer Fourier transform infrared spectrometer (FT-IR) with Universal ATR Sampling Accessory was used to characterize the precursor polyimides and TR-PBO films. In addition, FT-IR was used to prove the conversion of the precursor polyimide films into PBOs. The scan range was from 4000 to 650 cm^{-1}. Inherent viscosities of polyimide precursors were evaluated at 30 °C using an automated Canon-Ubbelohde suspended level viscometer with NMP as the solvent. The polymer concentration was 0.5 g/dL in every case.

The glass transition temperatures (T_g) of the polyimide films were determined by modulated temperature differential

scanning calorimetry (MDSC) analyses on a TA Q-2000 calorimeter (TA Instruments, DE, USA). MDSC allows separation of the *reversing* contribution to the average heat flow (attributed to the heat capacity), as well as the *non-reversing* contribution to the average heat flow (attributed to the kinetic effects such as enthalpy recovery or recrystallization). The temperature calibration was performed by taking the onset of the endothermic melting peak of several calibration standards: octane (T_m = 217.26 K), indium (T_m = 430.61 K) and zinc (T_m = 693.38 K). The organic standard was a high-purity Fluka product, while the metal standards were supplied by TA Instruments Inc. Enthalpy was calibrated using Indium (melting enthalpy $\Delta_m H$ = 28.71 J g^{-1}). The module of the complex heat capacity was calibrated by measuring sapphire in the studied temperature range and the frequencies of modulation used during experimentation. A heat ramp rate of 5 °C min^{-1} up to 450 °C was used with a modulation period of 40 s and a temperature amplitude modulation of 1.5 °C. T_gs were attained from the *reversing* heat flow signal.

Thermogravimetric analyses (TGA) were conducted on a TA Q-500 thermobalance (TA Instruments), combined with a mass spectrometer (MS) ThermoStar™ GSD 301T (Pfeiffer Vacuum GmbH, Germany). Dynamic ramp scans were run at 10 °C min^{-1} to find out about thermal stability characteristics as well as the thermal rearrangement from 60 to 850 °C. Furthermore, isothermal thermogravimetric analyses were carried out in order to adjust for the most appropriate thermal treatment settings for TR films preparation and to estimate the percent conversion of polyimide precursors to the final TR-PBOs. Polyimide film samples, thermally treated at 300 °C, were heated to the selected rearrangement temperature (350 °C, 400 °C or 450 °C) at a heating rate of 5 °C min^{-1} and held isothermally for 3 h. The nitrogen purge gas was used (60 mL min^{-1}) and the sample mass was approximately 5 mg.

Intermolecular distances of the PI precursor membranes and TR-PBO membranes were determined by wide angle X-ray scattering (WAXS) experiments performed in reflection mode at room temperature with a Bruker D8 Advance system fitted with a Goebel mirror and a PSD Vantec detector. A Cu-*Kα* (wavelength L=1.542 Å) radiation source was used. A step-scanning mode was employed for the detector from 2-55°, with a 2θ step of 0.024° and a scan rate of 0.5 s per step. The average *d*-spacing was obtained from the Bragg's equation:

$$n\lambda = 2d \, sin\theta \qquad (2)$$

where *d* is the *d*-spacing, θ is the scattering angle and *n* is an integer number related to the Bragg order.

Densities were determined with the Archimedes' principle using a XS105 Dual Range Mettler Toledo balance coupled with a density kit by weighing samples at room temperature, in air, and then in a liquid of known density (Isooctane, Sigma Aldrich, > 99%). The density of the sample was estimated from the expression:

$$\rho_{sample} = \rho_{liquid} \frac{W_{air} - W_{liquid}}{W_{air}} \qquad (3)$$

The density data were used to evaluate chain packing using the fractional free volume (*FFV*), which was calculated using the following relation:

$$FFV = \frac{V_e - 1.3 \, V_W}{V_e} \qquad (4)$$

where V_e is the polymer specific volume (cm^{-3}/mol) and V_W is the Van der Waals volume (cm^{-3}/mol), which was given by molecular modeling applying the semi-empirical method Austin Model 1 (AM1) [36] in the Hyperchem computer program, version 8.0 [37].

Gas permeation properties were determined using the *time lag* method with a barometric permeation instrument for single gas feeds at 30 °C. The downstream pressure was maintained below 10^{-2} mbar, while the upstream pressure was kept at 1 bar for all gases. Helium (He, 2.6 Å), oxygen (O$_2$, 3.46 Å), nitrogen (N$_2$, 3.64 Å), methane (CH$_4$, 3.8 Å) and carbon dioxide (CO$_2$, 3.3 Å), which was tested last to avoid any potential influences due to plasticization, were used in permeation experiments. The purities for CH$_4$ and O$_2$ were greater than 99.95% and all other gases were greater than 99.99%. Helium permeation tests at three upstream pressures (1, 3 and 5 bar) were carried out to verify the absence of pinholes. Gas permeability coefficients (*P*), which are usually expressed in Barrers [1 Barrer = 10^{-10} (cm^3 (STP) cm)/(cm^2 s cm Hg) = 7.5005·10^{-18} m^2 s^2 Pa^{-1} (SI units)], were obtained from the slopes in the steady state region of pressure increase as a function of time, according to the following expression:

$$P = \frac{273}{76} \frac{Vl}{ATp_o} \frac{dp(t)}{dt} \qquad (5)$$

where *A* (cm^2)*, V* (cm^3) and *l* (cm) are the effective area, the downstream volume and the thickness of the membrane, respectively, *T* denotes the temperature of the measurement in Kelvin, p_0 (cm Hg) refers to the pressure of the feed gas in the upstream compartment and (d$p(t)$/dt) (cm Hg/s) is the rate of pressure rise at steady-state. The ideal selectivity ($\alpha_{A/B}$) for components A and B was calculated from the ratio of permeability coefficients:

$$\alpha_{A/B} = \frac{P_A}{P_B} \qquad (6)$$

where P_A and P_B are the permeability coefficients of pure gases A and B, respectively.

Mechanical properties (uniaxial tension tests) were determined on a MTS Synergie 200 apparatus fitted with a 100 N load cell at room temperature. Samples, 5 mm wide and 3 cm long, were clamped at both ends with an initial gauge length of 10 mm. The elongation rate was held at 5 mm min^{-1}. At least eight samples were tested for each film.

Computer simulations were carried out by first drawing the molecules in Hyperchem [37] and then optimizing the molecular and intermediate structures at the AM1 level [36]. Subsequently, electronic energies of the optimized geometries were calculated by Density Functional Theory (DFT) (without any

geometrical constraint (use of Opt keyword) for starting molecules and final molecules) using the Becke's three parameter hybrid function [38] and the Lee *et al.* [39,40] correlation function with the 6-31G(d) basis set (B3LYP/6-31G(d)). For intermediates molecules, the structures obtained by AM1 were subsequently calculated using the Gaussian 03 and Gaussian 03W packages [41] with an energy job type (single point calculation). Additional data on the quantum-mechanical process for the conversion of *ortho*-hydroxypolyimides to TR-PBOs and also from *ortho*-hydroxypolyamides to β-TR-PBOs will be detailed in a coming report. Molecular depictions were created using the Arguslab 4.01 freeware program [42].

Results and discussion

Synthesis and Characterization of the Precursor Polyimides

Precursor polyimides were synthesized using a classical and quantitative two-step low-temperature polycondensation method in which the diamine, HAB or DMAB, was reacted with dianhydride 6FDA at room temperature in a polar aprotic solvent (NMP or DMAc). DMAc was selected for the chemical cyclodehydration reactions since it can be removed during the membrane formation step. However, for the azeotropic cycloimidization, NMP was used since the boiling temperature of DMAc is similar to that of *o*-xylene, which can hinder water release. High-viscosity poly(amic acid) intermediates, *HPAA* and *MeOPAA*, were obtained through a base-assisted *in situ* silylation method [43] that requires the use of a silylating agent (CMTS), Py and DMAP as activating reagents to increase the reactivity of the –NH₂ groups. In the second stage of the process, the poly(amic acid)s *HPAA* and *MeOPAA* were cyclized by different imidization methods depending on the desired final polyimide structure.

Azeotropic imidization was carried out adding *o*-xylene to form an azeotrope with the water produced during the ring-closure reaction. Accordingly, *HPAA* was azeotropically imidized to obtain *PI-OH* precursors. Chemical imidizations were accomplished by the addition of a mixture of acetic anhydride and Py to the *HPAA* and *MeOPAA* solutions. Without the use of a protecting group, the hydroxyl groups of the HAB moiety were converted to acetate groups during the imidization process and thus the acetate-containing polyimide, *PI-OAc*, was obtained.

PI-OH, *PI-OAc* and *PI-OMe* polyimides showed values of inherent viscosity of 1.51, 0.62 and 0.59 dL/g respectively, offering high enough molecular weights to be employed in the preparation of dense membranes with good mechanical properties. The yield of the polycondensation reactions was higher than 98 - 99 % for all polyimides produced.

The chemical structure of the precursor polyimides was confirmed by ¹H-NMR. Fig. 1 shows the NMR spectra for the three polyimides where the peak allocations have been included. As can be seen in the aromatic region, the hydrogens that correspond to the phenyl moieties of the diamine (b, c and d) are upshifted relative to the hydrogen peaks ascribed to the phenyl groups of the dianhydride (e, f and g). There was a similar chemical shift seen for all polymers, indicating that the

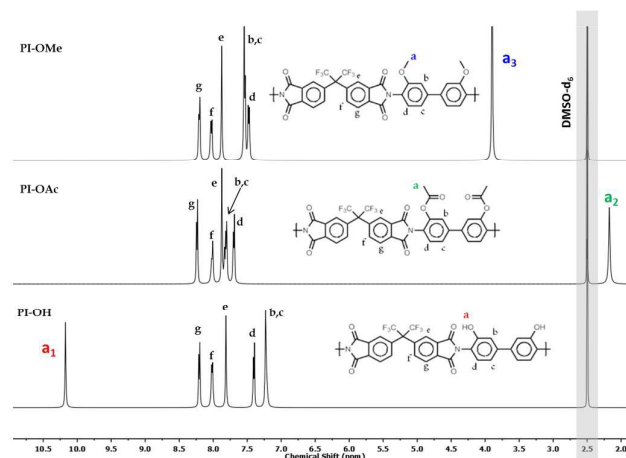influence of the electronic features of the diamine aromatic rings on the dianhydride ones was negligible.

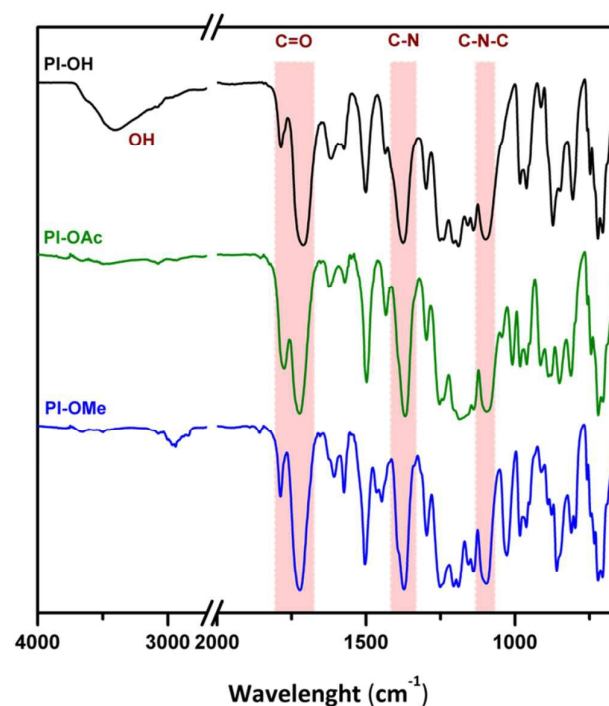**Fig. 1.** ¹H-NMR spectra of the precursor polyimides (DMSO-d_6, 500 MHz)

Fig. 2. ATR-FTIR spectra of precursor polyimide films.

The protons of the hydroxyl group (a₁) were observed at 10.23 ppm on the *PI-OH* spectrum while, for the *PI-OAc* and *PI-OMe* spectra, the peaks in the aliphatic region at 2.16 and 3.88 ppm corresponded to the methyl protons in the acetate group (a₂) and in the methoxide group (a₃), respectively. In addition, the absence of the OH peak at 10.23 ppm in the *PI-OAc* spectrum indicated that complete acetylation was achieved.

The IR spectra of polyimide films are shown in Fig. 2. All polyimides showed absorption bands at around 1780 cm⁻¹ (symmetric C=O stretching), 1720 cm⁻¹ (asymmetric C=O stretching) and at approximately 1375 cm⁻¹ (C-N stretching),

verifying the existence of imide moieties. In addition, absorption peaks at 1250 –1100 cm^{-1} were denoted as the C-F

stretching band of the hexafluoroisopropylidene moiety. In the

Table 1. Thermal Properties of Precursor Polyimide Films.

Polymer code	T_g (°C)[a]	T_{AP} (°C)[b]	T_{max} (°C)[c,d]	Theoretical wt. loss (%)	Measured wt. loss (%)[d]	T_d (°C)[d]
PI-OH	356	345	425	14.1	12.6	550
PI-OAc	278	282	397	24.3	13.0	546
PI-OMe	311	380	493	17.8	13.8	546

[a] Middle point of the endothermic step of the "reversing" contribution to the average heat flow during the first scan of MDSC measurements conducted at a heating rate of 5 °C/min, modulation period of 40 s and a temperature modulation amplitude of 1.5 °C, under a nitrogen atmosphere. [b] Apparent starting temperature at which first weight loss begins. [c] Temperature at the maximum point of the first weight loss. [d] Determined by TGA at a heating rate of 10°C/min under nitrogen atmosphere.
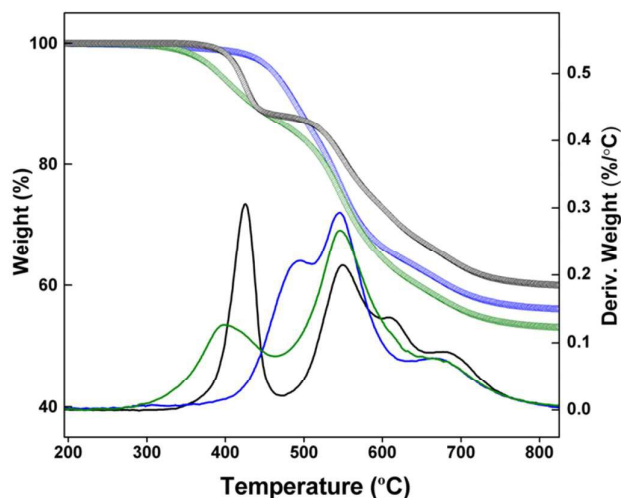

Fig. 3. Thermogravimetric analysis of precursor polyimide films at a heating rate of 10 °C min^{-1} under N$_2$ atmosphere; ● PI-OH, ● PI-OAc and ● PI-OMe

case of *PI-OH* pattern, the broad band in the region from 3200 – 3600 cm^{-1} was attributed to O-H vibrations on the phenolic groups.

Thermal Properties of Precursor Polyimides

The thermal characteristics of these three polyimides were evaluated using MDSC and TGA-MS techniques. As observed in MDSC (Fig. S1 in the *Supporting Information*), the glass transition temperature, T_g, was clearly affected by the *ortho*-positioned substituent. Thus, the *PI-OH* exhibited the highest T_g at 356 °C, whereas the non-hydroxylated polyimides showed a lower T_g of 278 °C and 311 °C for *PI-OAc* and *PI-OMe*, respectively (see Table 1). This displacement of the T_g to lower values for the non-hydroxylated polyimides can be attributed to the reduced ability to produce hydrogen bonds, and the higher free volume due to the presence of acetate and methoxy groups. The combination of both factors reduces the cohesive energy and consequently the glass transition temperature. A comparison of TGA and the first derivative

traces for all precursor polyimide films at 10 °C min^{-1} under a N$_2$ atmosphere can be seen in Fig. 3. *PI-OH* clearly shows two distinct weight loss steps, in agreement with previously reported data [28,44]. The first weight loss step, in the range of 300-500 °C, can be associated with the thermal rearrangement of *PI-OH* to the TR-PBO structure and the release of CO$_2$, as confirmed by TGA-MS analyses (Fig. 4). The second weight loss step is ascribed to the generalized decomposition of the *in situ* formed TR-PBO backbone at around 500-600 °C [28,44–46]. *PI-OAc* shows a similar TGA profile with two weight loss steps similar to that observed for *PI-OH*, suggesting that the thermal rearrangement to TR-PBO also took place for the polyimide. However, the apparent starting temperature of the first weight loss of *PI-OAc* was observed around 60 °C lower than that of *PI-OH* (see Table 1). In addition, the maximum weight loss rate (r$_{max}$) for the *PI-OH* film, analyzed from the differential TGA curve (DTG), was r$_{max}$=0.30%/°C, whereas a lower value of r$_{max}$=0.13%/°C was found for the *PI-OAc* film. It was difficult to discern the two-step weight loss for *PI-OMe* film (these steps could be seen in the differential curve), possibly due to the improved thermal stability given by the methoxy group or because of the existence of a different rearrangement mechanism. In this case, the apparent starting temperature for the first weight loss was observed at 380 °C, and the maximum weight loss rate (at 495 °C) was 0.22%/°C. Additionally, the measured weight losses for the *PI-OH*, *PI-OAc* and *PI-OMe* films were 12.6, 13.0 and 13.8 %, respectively. These values are lower than the theoretical values for full conversion to PBO (which would be 14.1, 24.3 and 17.8 %, respectively), assuming that the TR mechanism from *ortho*-substituted PI into PBO occurs in all cases. TGA-MS was used to identify the composition of the evolved gases from the film sample during the TGA scan. Fig. 4 shows that the molecular weight of the evolved products was between 10 and 70 amu, using the same experimental settings than those employed in the TGA experiment illustrated in Fig. 3. In the *PI-OH* film (a), mass components having molecular weights of 17, 18, 19, 20, 44, 51 and 69 amu were evolved during the full scan. As mentioned
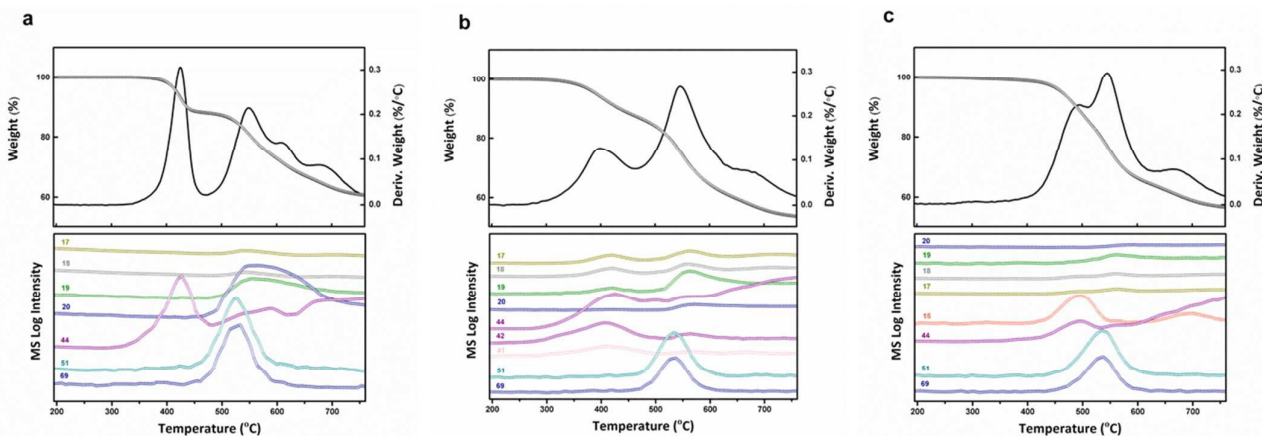
Fig. 4. Thermogravimetric analysis combined with mass spectroscopy (TGA-MS) of (a) *PI-OH*, (b) *PI-OAc* and (c) *PI-OMe* precursor polyimide membranes (heating rate of 10 °Cmin^{-1} under N_2 atmosphere).
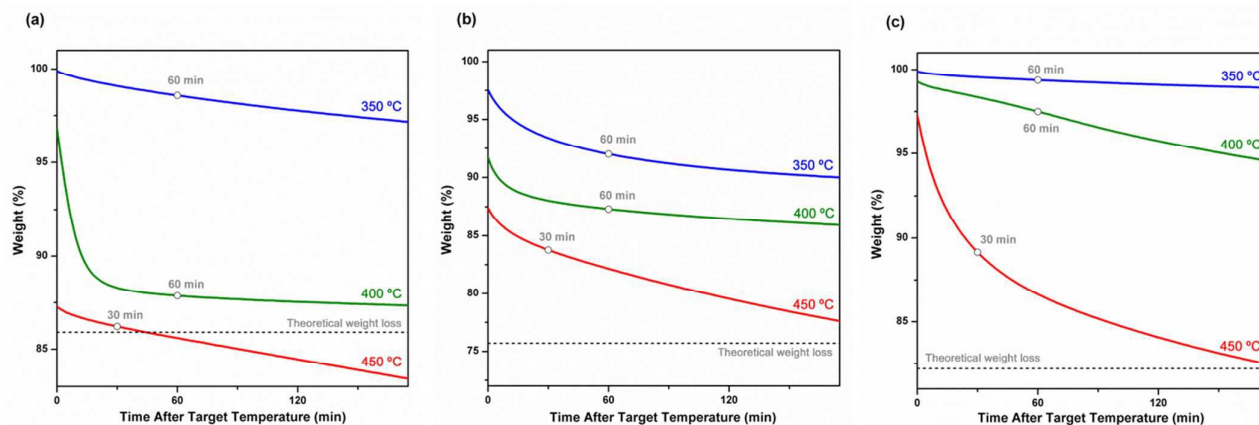

Fig. 5. Isothermal thermogravimetric analysis, under N_2 atmosphere, of (a) PI-OH, (b) PI-OAc and (c) PI-OMe precursors. This graph shows weight loss of these polyimides as a function of time at the indicated temperatures. Empty circles represent the conditions used for membranes employed in transport property characterization.

above, the first mass loss is attributed to the decarboxylation of the polyimide during thermal rearrangement; thus, as previous studies reported [47–49], only the peak associated with the molecular weight of 44 was observed below 450 °C. In the second stage, which is associated with polymer degradation, all of the other species were detected. Evolved MS products with 19, 20 and 69 amu, indicate the cleavage of groups containing fluorine atoms (trifluoromethyl) on the polymer backbone. These correspond to fragments of F, HF and CF_3, respectively [50]. The peaks associated with molecular weights of 17 and 18 amu indicate loss of water within the polyimide structure. Finally, the molecular weights of 44 and 51 can be attributed to the general degradation of the polyimide.

However, for the *PI-OAc* film, in addition to these molecular losses, other peaks can be observed in the thermal rearrangement region. The mass losses for molecular weights of 41 and 42 were attributed to loss of the acetate groups in the form of a ketene moiety [51]. Moreover, molecular weights of 17 and 18, corresponding to H_2O, were also detected in the first step, which could plausibly indicate that chemical imidization was not complete for this case [52]. In the *PI-OMe*, in the first weight loss region, along with the peak associated with CO_2, a change in intensity was observed for species having a molecular weight of 15, which could be associated with the loss of methyl groups resulting from the methoxy group breakage [53,54].

Journal Name

ARTICLE

Table 2. Physical Properties of Precursor Polyimides and Their Corresponding TR Membranes

Polymer code	Conversion[a] (%)	Density (g cm^{-3})	FFV	Increment in FFV (%)	d-spacing (Å)
PI-OH	0	1.458	0.160	–	5.57
TR-OH350	11	1.453	0.159	–	5.71
TR-OH400	86	1.373	0.176	10	6.06
TR-OH450	96	1.337	0.194	21	6.14
PI-OAc	0	1.413	0.170	–	6.11
TR-OAc350	33	1.429	0.154	–	6.05
TR-OAc400	52	1.391	0.172	1	6.30
TR-OAc450	67	1.345	0.196	15	6.51
PI-OMe	0	1.388	0.174	–	5.99
TR-OMe350	4	1.376	0.181	4	6.16
TR-OMe400	14	1.360	0.191	10	6.20
TR-OMe450	61	1.322	0.214	23	6.36

[a]PI transformation for the different series after 60 min at 350 °C and 400 °C and 30 min at 450 °C

Thermal Treatment of Precursor Polyimides

Supplementary TGA analyses were performed to adjust the thermal treatment settings for TR sample preparation in the tubular furnace. To do this, the PI films treated at 300 °C were further heated to the desired temperature (350 °C, 400 °C and 450 °C) using a heating rate of 5 °C min^{-1}, and then held isothermally at the target temperature for 3h. Fig. 5 depicts the isothermal thermograms for *PI-OH*, *PI-OAc* and *PI-OMe* precursor films, showing weight loss as a function of time after reaching the desired rearrangement temperature. The conversion percentage of the precursor polyimide films into the assumed final TR membranes was evaluated based on data obtained from isothermal thermograms using Equation 7:

$$\% \ Conversion = \frac{Experimental \ Mass \ Loss}{Theoretical \ Mass \ Loss} \times 100 \qquad (7)$$

This theoretical CO_2 loss, which is 14.1 % for *PI-OH*, 24.3 % for *PI-OAc* and 17.8 % for *PI-OMe*, is shown as a dashed line in the figure.

Conversion values for the precursor polyimides are shown in Table 2. According to previous studies [28,45,55] the thermal cyclization reaction is very sensitive to the applied temperature, showing acceleration in the thermal rearrangement kinetics with increasing temperature. As can be seen, the amount of weight loss increases as a function of rearrangement temperature and time, for all cases. For the *PI-OH* film, at 350 °C, the weight loss was low at all heating times (11 % in 1 h), whereas it notably increased at 400 °C reaching its maximum value (96 % in 1 h) at 450 °C, exceeding the theoretical weight loss for longer treatment times. However,

the *PI-OAc* film achieved higher weight losses than *PI-OH*, (33 % in 1 h) at 350 °C presumably due to its lower T_g that favors the start of rearrangement at lower temperatures, as can be seen in Fig. 3. At 400 °C and 450 °C, the weight loss gradually increased, potentially reaching the theoretical value for treatments longer than 3 h at 450 °C. For the case of *PI-OMe*, the weight loss was quite low for all heating times both at 350 °C (4 % in 1 h) and at 400 °C (14 % in 1 h). As the T_g of this polymer is also significantly lower than that of *PI-OH*, the lower reactivity of this PI should be related with the different behavior of the OMe group, as has been indicated previously in the dynamic TGA curves. At 450 °C, in the *PI-OH* film, the weight loss notably increased, but the value did not surpass the theoretical weight loss for the first 3 h, reaching a value of 61 % in 30 min. Presumably, using a longer thermal treatment would result in a higher percentage of conversion and, consequently, in higher *d*-spacing values, which would translate into a higher degree of *openness* within the polymer matrix.

In order to have thermal histories similar to those reported in other studies related to TR materials, the residence times chosen for thermal treatment were 1 h for both 350 °C and 400 °C, and 30 minutes for 450 °C (represented by empty circles in Fig. 5). Thus, the polyimide precursors, *PI-OH*, *PI-OAc* and *PI-OMe*, were thermally treated in a tubular furnace following the chosen protocols.

The effect of the thermal treatment on polymer chain packing, which has a considerable influence on the gas separation properties, was explored by wide-angle X-ray diffraction (WAXD). In Fig. S2 (*Supporting Information*), the X-ray patterns, measured at room temperature, of thermally treated
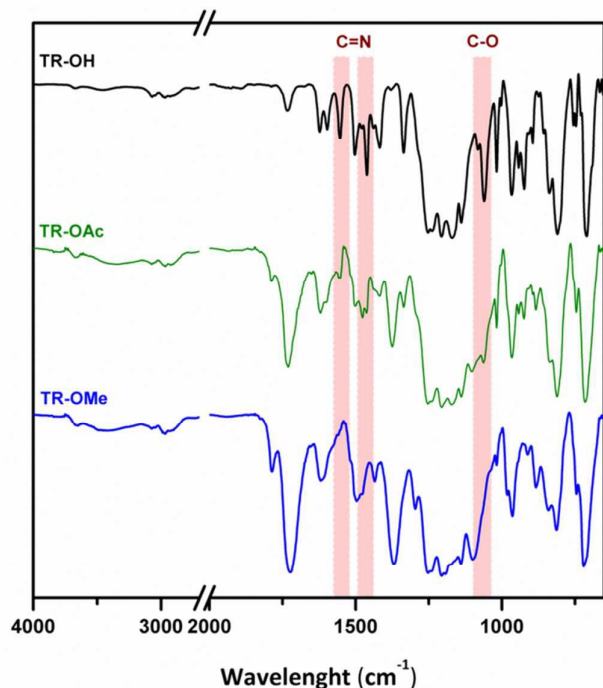
Fig. 6. ATR-FTIR spectra of films thermally treated at 450 °C for 30 minutes

membranes and polyimide precursor films are compared. All of the membranes were in a completely amorphous state, proved by the presence of an amorphous halo. The most probable intersegmental distance (*d*-spacing) values were estimated according to Bragg's equation, and data are shown in Table 2. The precursor polyimides, *PI-OH*, *PI-OAc* and *PI-OMe*, showed preferential intersegmental distances with values of 5.57, 6.11 and 5.99 Å, respectively, whereas films treated at 450 °C resulted in a larger intersegmental distances, with values of 6.14, 6.51 and 6.36 Å, respectively. For the other treatments, a linear change was observed. Accordingly, the use of thermal treatments led to higher intersegmental distances, which was in agreement with other TR polymers previously studied [28,45,47].

Density data are also compiled in Table 2. It was observed that the density of the polyimide precursor films was higher for *PI-OH* due to its ability to create hydrogen bonds; these give rise to a more densely packed polyimide structure. As expected, thermally treated membranes showed lower densities as thermal treatment temperature increased, excluding the TR-OAc350 membrane, which showed a slightly higher density than its precursor membrane, *PI-OAc*.

The Van der Waals volumes, V_W for partially converted samples, were calculated using Equation 8, which considers the degree of conversion of the polyimide precursor into the final TR structure, where the value c is the fractional mass conversion determined as the quotient of the experimental mass loss measured by TGA and the theoretical mass loss required to achieve 100 % conversion. $V_{W,TR}$ and $V_{W,PI}$ values refer to the Van der Waals volume of TR and PI structures, respectively. These Van der Waals volumes were introduced in

Equation 4 in order to achieve the FFV values of the partially converted structures.

$$V_W = c\,V_{W,TR} + (1-c)V_{W,PI} \qquad (8)$$

The changes that occurred to the structure of the precursor polyimides after thermal treatment in the tube furnace were analyzed using ATR-FTIR. Complete details of these structural changes can be seen in the *Supporting Information* (Fig. S3), where the ATR-FTIR spectra for all thermally treated samples as well as for polyimide precursors are shown. Fig. 6 shows the ATR-FTIR spectra of the films thermally treated at the highest temperature (450 °C) for 30 minutes. As can be seen, in the TR-OH sample spectrum, the appearance of intense peaks at wavenumbers around 1557, 1465 and 1060 cm^{-1}, which are characteristic of the PBO structure, confirmed that the *PI-OH* film undergoes a thermal rearrangement into PBO. In addition, the intensity of the imide peaks at 1780, 1720, 1375 and 1102 cm^{-1}, and the strong and broad absorption band from the hydroxyl group around 3400 cm^{-1}, were found to substantially decrease. In the TR-OAc spectrum, the representative peaks for PBO could also be observed, even though they were less intense when compared with the TR-OH sample, suggesting the existence of PBO in the final structure. In this case, the imide peaks partially decreased, and the emergence of a new strong band around 3400 cm^{-1}, which did not appear on the spectrum of the *PI-OAc* precursor, proved the presence of new OH phenolic groups. For the TR-OMe, the characteristic OH phenolic group peak appeared when the imide peaks decreased. However, as mentioned above, the polymer density decreased also for this polymer going from the starting material to the final one. This suggests that a structural change took also place, similar to the type underwent by *ortho*-hydroxypolyimides. It is well documented that the pyrolysis of methoxy aromatic compounds proceeds via the homolytic scission of the (H$_3$C)-O linkage, with the subsequent loss of CH$_3$ groups in the form of methane or ethane followed by the recombination of the phenoxy radical to phenol [56]. If this mechanism is accepted as a first step in the transformation, *ortho*-methoxypolyimides would then render TR-PBOs in the same way as *ortho*-hydroxypolyimides do. However, the identification of the final material, TR-OMe450, by FT-IR did not entirely agree with this assumption, as a clear transformation into PBO was not confirmed from spectral analysis. As discussed above, the strong carbonyl bands of imide C=O stretching at around 1715 and 1785 cm^{-1} persisted in a great extent after heating at 450 °C for 30 minutes, contrarily to what happens on heating *ortho*-hydroxypolyimides. This seems contradictory with the suggestion that the most probable first step of the thermal treatment is the loss of methyl groups and the subsequent formation of phenols or phenol radicals, with almost simultaneous formation of *ortho*-hydroxypolyimide. Thus, the persistence of the intense imide peaks and the non-appearance of the characteristic PBO bands seem to indicate that thermal rearrangement did not occur via the accepted *TR-PBO* process.

This spectroscopic evidence moved us to search for a plausible route and settle the mechanism governing the thermal rearrangement undergone by *ortho*-methoxypolyimides. Upon reviewing the spectral data reported for TR-PBOs in the last years, two points appear most significant: 1) there is general agreement of the mechanism proposed by Tullos *et al.* for the thermal rearrangement of *ortho*-hydroxypolyimides to TR-PBOs [30,44,57–60], although there is not full agreement about the effect of the precursor synthesis route (chemical imidization, azeotropical imidization or direct thermal imidization) on the composition of the final TR-PBO [47,61–63], and 2) when starting from *ortho*-esterpolyimides the composition of the final material is far from a neat PBO as strong spectral evidence speaks to the prevalence of polyimides or other groups having comparable IR signals [58,64]. In fact, if one reviews the attempts made to use *ortho*-esterpolyimides (mainly *ortho*-acetylpolyimides) instead of *ortho*-hydroxypolyimides as precursors for TR-PBOs, it can be seen that the possibility of an alternative mechanism was obviated and authors focused their research effort mainly on studying the advantages of using *ortho*-esters for better solubility, improved *FFV* (splitting off of aliphatic rests should help increase the amount of regular microcavities) or lower T_g, which could favor a drop in the rearrangement temperature. As a rule, the final heated films of the supposed TR-PBOs exhibited strong IR bands corresponding to aromatic imides or other chemical groups having similar bands, and the authors did not pay attention to this experimental evidence. Thus, another mechanism, or a parallel one, could be responsible for the final chemical composition shown by IR spectra in those cases where *ortho*-hydroxypolyimide is not the precursor.

Kostina *et al*. recently reported a thorough study clearly addressing the mechanisms that govern the molecular transformations undergone by *ortho*-hydroxypolyimides at temperatures over 400 °C [32,65]. They postulated that the formation of rigid aromatic lactams, not only polybenzoxazoles, is responsible for the series of conformational changes that lead to the observed strong effects on physical properties, particularly the dramatic increase in fractional free volume and hence gas diffusivity. In those papers, and based on spectroscopic signals, the observed loss of CO_2 was ascribed to the formation of lactams (phenanthridin-6(5H)-one moieties) through thermal decomposition of an intermediate lactam-lactone (6H-dibenzo[b,f][1,4]oxazocine-6,11(12H)-dione units). This assumption was supported by quantum chemical calculations that suggest that the formation of lactams is energetically more favorable than the formation of benzoxazoles. Nonetheless, it can be presumed that by applying the very high temperatures used to force intramolecular rearrangement, both lactams and benzoxazoles can be formed, and that the final composition is greatly affected by the final temperature and the heating protocol. It must be remarked that there is spectroscopic indication of the persistence of polyimide, apart from the merging of the bands attributable to lactams, as the characteristic IR bands of imide at about 1778, 1720, 1550 and 725 cm^{-1} remain in the IR spectra reported by Kostina *et al.*,

and this is the case for most TR-PBOs prepared from *ortho*-esterpolyimides reported up till now [32,65].

Thus, it seems that, although *ortho*-hydroxypolyimides do lead mostly to TR-PBOs by thermal rearrangement, the thermal treatment of other related precursors, like *ortho*-esterpolyimides or *ortho*-methoxypolyimides, do not follow the same rearrangement paths and therefore the resulting material after heating to 450 °C is far from a neat polybenzoxazole. The presence of lactam, lactone-lactam and benzoxazole can be detected in various proportions depending on: 1) the nature of the precursor, 2) the synthetic method applied to prepare the precursor and 3) the schedule followed in the final heating step. Furthermore, in the particular case of TR polymers attained from *ortho*-methoxypolyimide, benzoxazole units should be present in a relatively small amount as spectral data does not support their presence in significant amounts. So, a mechanistic path is proposed in this paper detailing the process of thermal treatment at high temperatures in solid-state *ortho*-methoxypolyimides. This mechanistic explanation is far from thoroughly justified and additional work in this topic will be carried out using other techniques like solid-NMR, XPS and FTIR-MS. This study will be published in the near future. Based on our work in TR materials, the mechanistic path we propose will be similar to the one described in Scheme 1.

Herein, we postulate that the final molecular moieties arising from thermal treatment depends on the group attached to the *ortho* position of the amino group. When the group is OH (3), the high temperature results in conversion to TR-PBO (5) or the formation of (4) by homolytic breakage of the O-H bond.

When the model having an acetyl group (2) is considered, a predominant loss of ethenone (ketene, $CH_2=C=O$) is observed, as evidenced by TGA-MS, with formation of (3 or 4). This ethenone group (m+=42 amu) is formed by the decomposition of the –(OCO) bond with the formation of the acyl group and breakage of this group to ethenone and a proton. However, when the methoxy group is considered, TGA-MS indicates the loss of methyl groups (m+=15 amu), which results in the formation of (4). Evidently, (3) can be converted to (4) and (4) to (3) by losing or gaining an H, respectively. The published works and the results of this paper seem to clearly point to the formation of the benzoxazole moiety being most favored by the OH precursor, slightly favored for the OCOCH$_3$ precursor, and less favored by the precursor having the OCH$_3$ group. Therefore, the reaction from (4) to (5) is not favored and it could be assumed that the presence of H (H+ or H·) entities in the medium should influence the rearrangement process. Thus, when the amount of H is high (OH polyimide), the classical TR rearrangement is the most favored and benzoxazole moiety formation is evident. However, the production of H moieties is small when the methoxy group is considered and consequently PBO formation is scarce. For the acetyl polyimide, mixed formation of both (3) and (4) intermediates could explain the observed FTIR results.

At this point, two questions arise from this assumption: 1) What is the role of H entities in PBO formation? and 2) Why
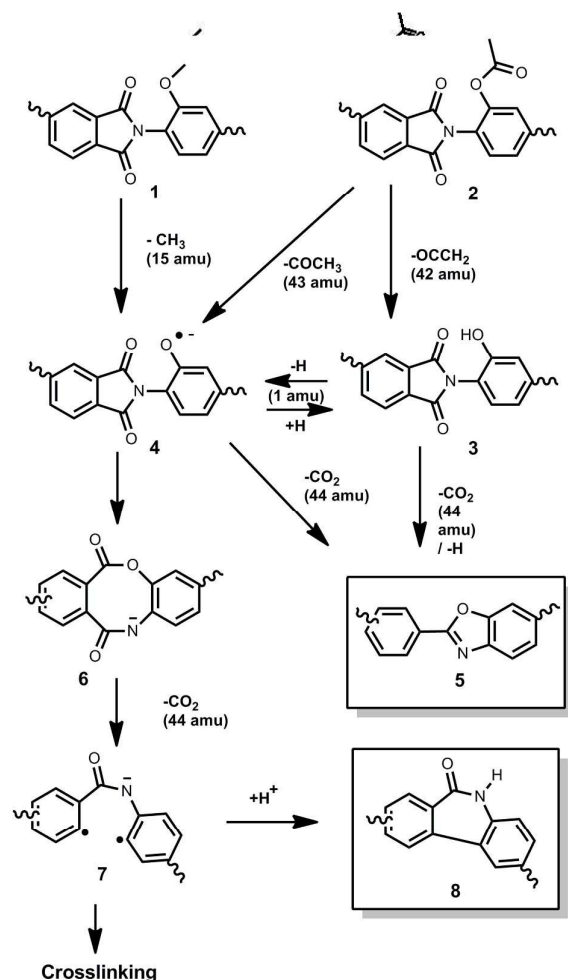
Scheme 1. Possible rearrangement mechanisms and final reaction products obtained by thermal treatment of *ortho*-hydroxy, *ortho*-methoxy and *ortho*-acetyl polyimides.
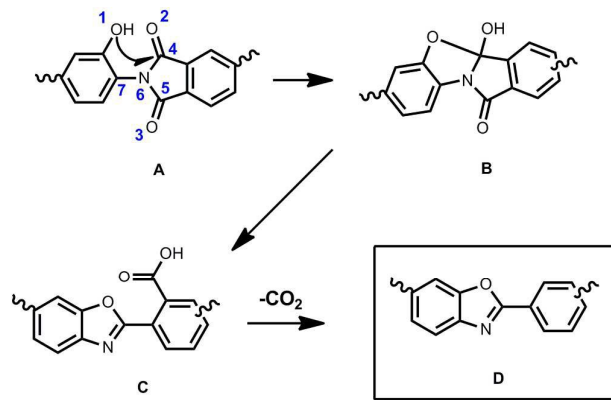
Scheme 2. Reaction mechanism proposed for the thermal rearrangement mechanism of PI-OH to TR-PBO

In response to question 1, the role of the proton could be ascribed to the protonation of some nucleophilic groups, which could produce an intermediate state that permits the preferential formation of the molecular moieties described in the Scheme 1. It seems to be accepted in the literature that the intermediate moiety formed during the conversion from *ortho*-hydroxypolyimide to polybenzoxazole is the B molecule described in Scheme 2. The formation of intermediate B seems to be evident, and hence many authors consider this moiety to be essential for achieving the final benzoxazole. However, molecular simulation calculations denote that the distance from the nucleophilic center (O1 of the OH moiety after the breakage of the O-H bond) to the carbonylic centers of the imide group (C4 or C5) in molecule A is significantly larger than 2.8 Å and a strong conformational change has to take place to permit this attack. However, it is plausible to consider that, at high temperature, a proton is able to jump from the OH group to some of the nucleophilic centers of the imide (see Scheme 3).
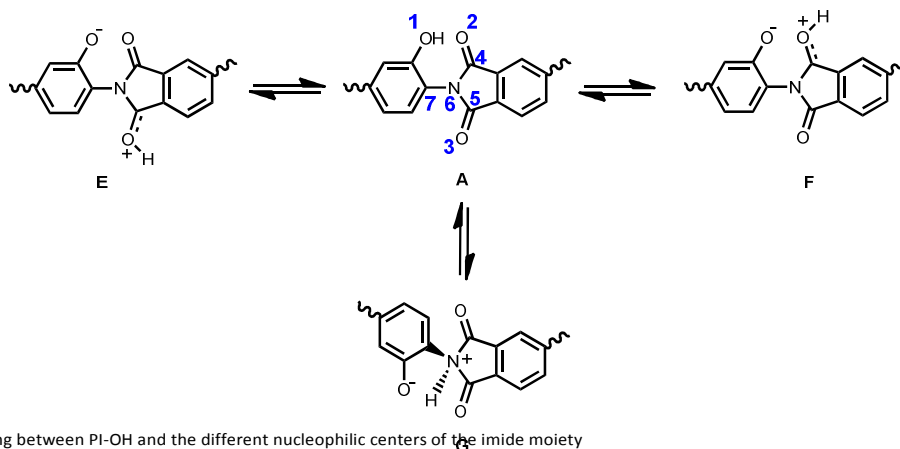
Scheme 3. Proton jumping between PI-OH and the different nucleophilic centers of the imide moiety
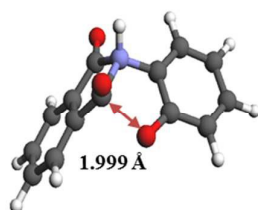
Journal Name

ARTICLE

Fig. 7. Structure of the *ortho*-hydroxypolyimide after the transfer of one proton from the OH group to the nitrogen imide moiety (intermediate G in **Scheme 3**), showing the required conformational change and the significant shortening of the distance between O1 and C4 or C5.
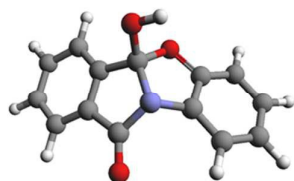

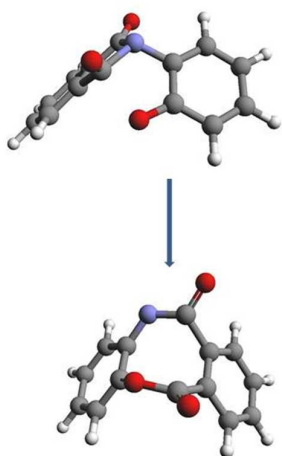**Fig. 8**. Intermediate molecule B formed from intermediate G (**Scheme 3**)

Fig. 9. Initial (up) and final step (bottom) of the reaction of deprotonated (O2 atom is no protonated) intermediate G (**Scheme 3**) to (lactone-lactam).

When one of the two oxygen atoms of the imide group is protonated by the transfer of a proton from O1 to O2 or O3 (structures E and F) an increase in the molecular energy is observed. No changes, however, are observed in the distance between the O1 and the carbonylic atoms C4 or C5 (the possible value for an eclipsed conformation is higher than 2.8 Å) and consequently the geometry of the protonated molecule

does not favor the attack on the carbonylic centers. Nevertheless, when the proton is transferred from O1 to the nitrogen of the imide group (N6) (structure G), an important conformational change takes place and the nitrogen adopts a pyramidal (sp^3) conformation. As a consequence of the new nitrogen conformation, the distance from O1 to C4 or C5 is significantly shortened (distance close to 2.00 Å) in such a way that the nucleophilic attack is plausible. Fig. 7 depicts the structure of protonated intermediate G showing the shortest distance between O1 and C4 or C5 that can be attained when the structure is allowed to rotate around the bond N6-C7. Additional protonation of the OH group (O2) on B, shown in Fig. 8, results in the release of a water molecule by breaking the O2-C4. Afterwards, the system evolves benzoxazole groups through the jumping of the hydrogen placed on N6 to the O2, thus forming bi-intermediate state B (Fig. 8). Evolution of this intermediate state by reaction of water on C5 gives the 2-carboxy benzoxazole, C moiety, which after losing a CO_2 molecule is converted to the final benzoxazole D (Scheme 2). When no hydrogens (protons (H+) or hydrogen radicals (H·) are involved in the reaction path, several steps of the proposed mechanism are not possible. However, the reaction could progress by thermal activation of A (Scheme 3). Thus, the formation of an eclipsed conformation can be achieved by bending the N6-C7 bond of (4) (Scheme 1), which should be favored at high temperature. This conformation permits the attack of O1 on C4, allowing the system to spontaneously form the lactone-lactam moiety. This spontaneous reaction has been seen in computer simulations. In fact, if the deprotonated structure in Fig. 7 is minimized by AM1, it spontaneously gives way to the lactone-lactam unit, as shown in Fig. 9. The ulterior decarboxylation of the lactone-lactam forms the proposed lactam. However this decarboxylation also produces a high amount of radical centers, which lead to a massive amount of crosslinking. This crosslinking process is always observed in TR materials, due to the high temperatures employed to convert the precursor polyimides to the final material. It should be noted that some of the excellent properties associated to TR-polymer; low physical aging, high resistance to plasticization and elevated chemical and thermal resistance could be explained by the high amount of crosslinked moieties present in these materials.

Finally, the high *FFV* of materials made from *ortho*-methoxy polyimides can be explained by existence of a large amount of eclipsed and bent conformation associated with the transitory molecule resultant of the deprotonation of structure G (molecular depicting placed in the up part of Fig. 9), which is required to produce the attack that leads to the lactone-lactam structure. Also, it should be commented that the

ARTICLE

lactone-lactam moiety has a contorted conformation, which could impart an excess of free volume to the material.

Table 3. Mechanical Properties of Precursor Polyimide Films and Their Corresponding Thermally Treated Membranes.

Polymer code	Tensile strength (MPa)	Elongation at break (%)	Modulus (GPa)
PI-OH	166	19.5	2.5
TR-OH350	167	15.9	2.7
TR-OH400	127	14.4	1.8
TR-OH450	27	1.7	1.8
PI-OAc	169	9.8	2.9
TR-OAc350	126	5.3	3.0
TR-OAc400	64	2.8	2.8
TR-OAc450	33	1.9	2.1
PI-OMe	176	7.5	3.0
TR-OMe350	179	8.8	2.7
TR-OMe400	146	8.7	2.3
TR-OMe450	56	3.6	1.8

Mechanical Properties

Mechanical properties were determined for all polymeric films studied in this work (precursor and thermally treated materials) and are shown in Table 3. Mechanical properties of the precursors were excellent with elastic moduli above 2.5 GPa, tensile strength higher than 150 MPa and good values for elongation at break. The mechanical properties of the membranes thermally treated at 350 °C did not appreciable change, except for the *PI-OAc* membranes, probably due to the premature thermal rearrangement that was observed by thermogravimetric analysis. The thermal treatment at 400 °C led to a slight decrease in mechanical properties, which was greater for the membrane derived from *PI-OAc*. However, the membranes from *PI-OMe* and *PI-OH* showed comparable mechanical properties when compared with other aromatic polymers. It should be noted that a detailed study of mechanical properties for TR materials has not been carried

out and only a few papers have dealt with this issue. Calle *et al.* [55] obtained TR derived from ether-benzoxazole units that showed mechanical properties lower than these obtained in this work for samples thermally treated at 400 °C. Li *et al.* [66] developed a class of TR with excellent mechanical properties, but the precursor had a high *FFV* and the conformational changes associated with thermal rearrangement were favored and it was found that elongation values were clearly higher than for any TR materials obtained so far. The mechanical properties for the samples treated at 450 °C dropped in all cases, and consequently, a decrease between 25-40 % was observed for all mechanic moduli. However, the reduction in tensile strength was significantly higher, with decreases between 70 and 80 % when compared with reference polyimides. Again, and common for TR materials, the elongation values were lower than 5 %. The best balance in mechanical properties for these materials was found with the TR-OMe450 sample. In conclusion, it could be stated that the thermal treatment of TR membranes from *PI-OMe* gave materials with mechanical properties able to withstand the high pressures employed in industrial gas separation applications.

Permeation Properties

Gas transport properties of the produced *ortho*-substituted polyimides and their corresponding TR-polymers were investigated for He, O_2, N_2, CO_2 and CH_4 gases and the results are presented in Table 4. The gas transport values measured for the thermally untreated precursors were permeability, which were typical values, considering the linearity of the polymers and their chemical composition. Moreover, the substituent seems to play a role on the permeability of the *ortho*-substituted polyimides, which can be related to the effect of the substituent on the *FFV*. Thus, the permeability is higher for *PI-OMe*, which has the higher *FFV* (0.174), followed by *PI-OAc*, with *FFV*: 0.170 and finally, *PI-OH* (0.160).

Table 4. Gas Permeation Properties of Precursor Polyimides and Thermally Treated Membranes.

Polymer code	Permeabilities (Barrers)					Ideal selectivities	
	He	N_2	O_2	CH_4	PCO_2	$\alpha_{O2/N2}$	$\alpha_{CO2/CH4}$
PI-OH	46	0.35	2.3	0.16	10	6.6	63
TR-OH350	70	0.59	3.8	0.29	16	6.4	55
TR-OH400	94	2.3	12	1.5	57	5.2	38
TR-OH450	200	10	45	7.7	240	4.5	31
PI-OAc	43	0.44	2.5	0.2	12	5.7	60
TR-OAc350	75	1.1	6.1	0.48	27	5.5	57
TR-OAc400	178	5.9	29	3.2	159	4.9	50
TR-OAc450	348	28	114	21	632	4.1	31
PI-OMe	56	0.68	4.1	0.31	20	6.0	65
TR-OMe350	75	1.1	6.1	0.48	28	5.5	58
TR-OMe400	118	3.0	14	1.6	78	4.7	49
TR-OMe450	328	23	93	18	540	4.0	30

Journal Name

ARTICLE

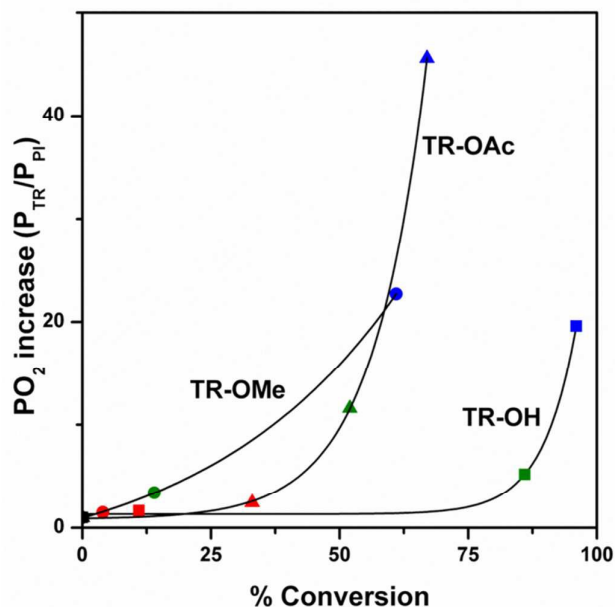**Fig. 10.** Plot of oxygen permeability increase (P(O$_2$)TR/P(O$_2$)PI) vs % conversion, based on a full rearrangement of PI to PBO or to poly(lactam). Red: 350 °C, Green: 400 °C, Blue: 450 °C

As mentioned previously above, the TR process for the different *ortho*-substituted polyimides does not take place at the same temperature and, moreover, the conversion, at the intermediate steps and at the final one, is also different in the three cases. Fig. 10 shows, at different treatment temperatures, the oxygen permeability increase versus conversion during the transition from the polyimide structure to PBO (the observed behavior is analogous for the other gases). As can be seen, different performances values are observed depending on the structure of the polyimide precursor. When the precursor is PI-OH, it is clear that the thermal process seems to lead to the conversion of the polyimide to polybenzoxazole where the weight loss corresponds to the release of fragments with 44 amu (CO$_2$). Therefore, the permeability increase can be accurately correlated with weight loss, with the PBO conversion and with the *FFV* change. In this case, the permeability increase seems to be somewhat low, mainly in the first steps of the process, when this parameter correlated with the PBO conversion. A large increase in permeability is achieved when the PBO conversion reaches values greater than 80% (5-fold increase in permeability when the PBO conversion goes from 0% to 86%) reaching a 20 times increase when the PBO conversion is near complete (96%). For the *PI-OAc* precursor, there is a sudden

increase in permeability that starts at approximately 40 % conversion, reaching a 12-times increase at 52% conversion, while the highest permeability increase (46-fold) is achieved when PBO conversion is only 67%. However, the formation of PBO from *PI-OAc* is not the only way to explain the effects of the thermal treatment. The TGA experiments demonstrate that there is a previous release of ketene and/or acetyl moieties (42 and 43 amu, respectively) that causes an increase in *FFV* due to the elimination of relatively bulky side groups, even if no TR process takes place at this temperature. After this loss, the resultant macromolecular structure can undergo thermal rearrangement to PBO (on releasing CO$_2$, 44 amu), form lactam (also on releasing CO$_2$, 44 amu) and form (lactone-lactam) moieties (with negligible weight loss; H, 1 amu). In this last case, the conversion to lactone-lactam cannot be evidenced by TGA measurements even though the formation of this structure could produce changes in *FFV* due to the existence of important conformational changes. In this context, molecular simulation calculations determined that the structural unit of PBO has a molecular volume of 415.8 A^3 whilst the molecular volume of the lactam unit is slightly lower (408.7 A^3) and thus the increase in *FFV* for the last structure should be slightly higher. Regarding *ortho*-methoxy polyimides, as was summarized in Table 2, the conversion of TR-OMe350 and TR-OMe400 is significantly lower than those corresponding to TR-OH and TR-OAc polymers. This fact could be based on two complementary processes: 1) By TGA measurements it is clearly seen (Fig. 3) that the initial temperature during weight loss, and consequently of conversion from one structure to another one, is considerably higher in TR-OMe, and 2) the initial weight loss in TR-OMe corresponds to the elimination of a moiety smaller than that observed for *PI-OAc*, as it can be seen in Fig. 4c. This shows that in the first steps of thermal weight loss there is simultaneous release of CO$_2$ (44 amu) and CH$_3$ (only 15 amu). The 15 amu moiety obviously corresponds to the release of a methyl group derived from the methoxy moiety. Again, after this ether breakage, the resultant chain can follow the mechanism proposed for *PI-OAc*, and the formation of PBO, lactam and lactone-lactam can proceed.

In conclusion, related to the thermal treatment that gives the highest gas permeability values, at 450 °C, both TR-OAc and TR-OH membranes suffer a significant amount of thermal rearrangement and both experience a significant increase in permeability. However, the permeability increase in TR-OAc450 is much higher, despite the much lower conversion. This lower conversion is probably caused by the superposition of the two mechanisms presented in Scheme 1; that is, the

simultaneous formation of PBO and of poly(lactam)s or poly(lactone-lactam)s.
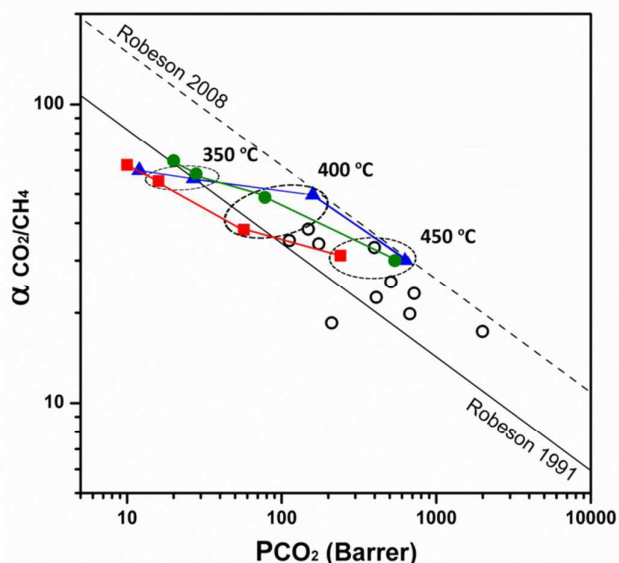

Fig. 11. Robeson plot for the three series of polymers: ■ TR-OH, ▲ TR-OAc, ● TR-OMe, ○ Literature data for TR. The temperatures of thermal treatment are shown in the plot.

The existence of the second mechanism, for the formation of polymers having lactams or lactone-lactam moieties, seems to justify the behavior of TR-OMe450 having the lowest conversion and also the lowest increase in permeability, since it did not suffer the sudden improvement observed in either of the other two cases. Therefore, the permeability behavior also seems to confirm the existence of a different rearrangement mechanism. Finally, it should be remarked that the lowest increase in permeability is partially counteracted by the highest permeability of *PI-OMe*, when compared with the other two precursors, and thus TR-OMe450 presents an excellent permeability-selectivity balance. In order to determine the gas permeability of membranes made in this work and also to figure out the effect of the thermal treatments, Robeson plots of permeability versus selectivity for some selected gas pairs were generated. For the O_2/N_2 gas pair, it was clearly observed that all membranes, pristine and thermally treated ones, placed below the 1991 Robeson limit. For the CO_2/CH_4 gas pair, results were more interesting (see Fig. 11). The thermal treatment at 350 °C produced an improvement for all the membranes that depended on the precursor. Thus, it was observed that the best gas separation properties corresponded to TR-OMe350 and TR-OAc350, which slightly overpassed the Robeson limit whilst the other one, TR-OH350, was below. The additional treatment at 400 °C resulted in an important increase in gas productivity in such a way that TR-OAc400 was placed near the 2008 Robeson limit. TR-OMe400 underwent an enhancement in gas separation properties although the permeability-selectivity plot was located between both limits. TR-OH400 kept well below the

1991 upper-bound. For this case, it should be noted that both substituted polyimides reached excellent values of gas productivity despite their low thermal rearrangement conversion. After the thermal treatment at 450 °C, all membranes were located clearly above the 1991 Robeson limit. However, TR-OMe450 was found to have experienced a significant improvement since this membrane was placed close to the 2008 upper-bound, placing it in the attractive zone for gas separation properties (high permeability while maintaining a good selectivity). After the thermal treatment TR-OAc450 showed the best permeability and selectivity trade-off.

Conclusions

Ortho-methoxypolyimides were successfully synthesized from 2,2′-dimethoxybenzidine and dianhydride 6FDA. Their treatment at high temperature, up to 450 °C, led to insoluble materials, whose IR spectra indicated a change in chemical composition. Significant changes in physical properties, particularly a dramatic change in permeation properties were also observed.

FTIR and TGA combined with mass spectrometry confirmed that methoxy groups were lost in a first weight loss step that started above 350 °C, and that a thermal rearrangement took place at higher temperature. Unlike *ortho*-hydroxypolyimides, *ortho*-methoxypolyimides did not seem to be converted into PBOs, the starting polyimide remained in a great proportion along even after the formation of benzoxazole and lactam units. Benzoxazoles and lactams appeared as a result of intramolecular recombination that occurred simultaneously at high temperature. This was unable to be quantitatively evaluated by FT-IR. Thus, there is still a lack of knowledge about the actual mechanism that governs the path from *PI-OMe* to TR polymers. In this work, based on the accepted mechanistic paths and also on recent literature, a plausible molecular simulation justification is proposed. In this explanation, the presence of protons or radical hydrogen atoms plays a critical role in benzoxazole formation. Also, the formation of (lactone-lactam) or lactam moieties was justified. Then, it is reasonable to presume that, at the high temperatures used during conversion, more than one rearrangement or recombination is possible. This leads to a final material that contains polyimide and moieties of both lactam and benzoxazole.

Gas permeation of the TR polymers reported here are attractive and compare fairly well with other TR-PBOs previously reported, exhibiting $P(CO_2)$ up to 540 Barrers and selectivities of 30 for the CO_2/CH_4 gas pair. Additionally, the permeability behavior seems to confirm the rearrangement mechanism proposed above, which yields mostly PBO structures in the case of TR-OH and a combination of PBO with poly(lactam) and poly(lactone-lactam) structures in the other two cases. The amount of poly(lactam) and poly(lactone-lactam) structures being higher in the thermally treated materials derived from *PI-OMe*.
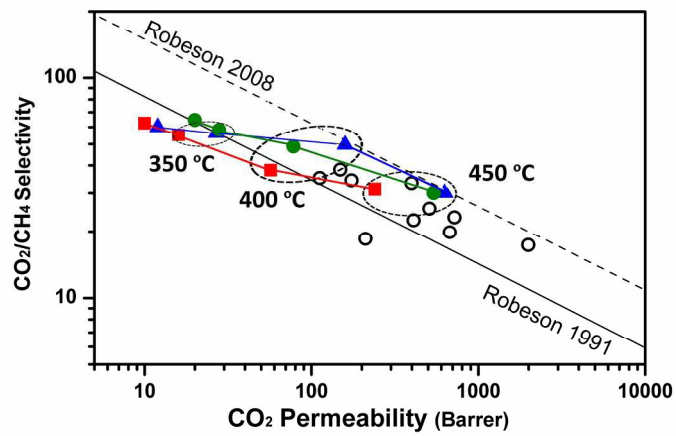
Acknowledgements

Notes and references

1   K. Ghosal and B. Freeman, *Polym. Adv. Technol.*, 1994, **5**, 673–697.
2   W. J. Koros and G. K. Fleming, *J. Memb. Sci.*, 1993, **83**, 1–80.
3   P. Bernardo, E. Drioli and G. Golemme, *Ind. Eng. Chem. Res.*, 2009, **48**, 4638–4663.
4   Y. Yampolskii and B. Freeman, *Membrane Gas Separation*, John Wiley & Sons Ltd., England,2010.
5   J. K. Adewole, a. L. Ahmad, S. Ismail and C. P. Leo, *Int. J. Greenh. Gas Control*, 2013, **17**, 46–65.
6   B. C. Bhide and S. A. Stern, *J. Memb. Sci.*, 1991, **62**, 13–35.
7   A. A. Belyaev, Y. P. Yampolskii, L. E. Starannikova, A. M. Polyakov, G. Clarizia, E. Drioli, G. Marigliano and G. Barbieri, *Fuel Process. Technol.*, 2003, **80**, 119–141.
8   S. Mokhatab and W. A. Poe, in *Handbook of Natural Gas Transmission and Processing (Second Edition)*, 2012, pp. 253–290.
9   B. D. Bhide and S. A. Stern, *J. Memb. Sci.*, 1993, **81**, 209–237.
10 S. Sircar, T. C. Golden and M. B. Rao, *Carbon N. Y.*, 1996, **34**, 1–12.
11 V. V. Usachov, V. V. Teplyakov, A. Y. Okunev and N. I. Laguntsov, *Sep. Purif. Technol.*, 2007, **57**, 502–506.
12 J. W. Phair and S. P. S. Badwal, *Sci. Technol. Adv. Mater.*, 2006, **7**, 792–805.
13 D. E. Jiang, V. R. Cooper and S. Dai, *Nano Lett.*, 2009, **9**, 4019–4024.
14 R. J. Lahiere, M. W. Hellums, J. G. Wijmans and J. Kaschemekat, *Ind. Eng. Chem. Res.*, 1993, **32**, 2236–2241.
15 M. Askari and T.-S. Chung, *J. Memb. Sci.*, 2013, **444**, 173–183.
16 M. Das and W. J. Koros, *J. Memb. Sci.*, 2010, **365**, 399–408.
17 C. Staudt-Bickel and W. J. Koros, *J. Memb. Sci.*, 2000, **170**, 205–214.
18 H. Herzog, *An Introduction to CO2 separation and capture technologies,* MIT Energy Laboratory Working Paper, Massachusetts Institute of Technology, 1999, 1–8.
19 X. Zhang, X. He and T. Gundersen, in *Energy and Fuels*, 2013, vol. 27, pp. 4137–4149.
20 L. M. Robeson, *J. Memb. Sci.*, 1991, **62**, 165–185.
21 B. D. Freeman, *Macromolecules*, 1999, **32**, 375–380.
22 C. H. Lau, P. Li, F. Li, T.-S. Chung and D. R. Paul, *Prog. Polym. Sci.*, 2013, **38**, 740–766.
23 N. Du, G. P. Robertson, J. Song, I. Pinnau and M. D. Guiver, *Macromolecules*, 2009, **42**, 6038–6043.
24 H. B. Park, C. H. Jung, Y. M. Lee, A. J. Hill, S. J. Pas, S. T. Mudie, E. Van Wagner, B. D. Freeman and D. J. Cookson, *Science*, 2007, **318**, 254–8.
25 S. Kim and Y. M. Lee, *Prog. Polym. Sci.*, 2015, **43**, 1–32.
26 H. J. Jo, C. Y. Soo, G. Dong, Y. S. Do, H. H. Wang, M. J. Lee, J. R. Quay, M. K. Murphy and Y. M. Lee, *Macromolecules*, 2015, **48**, 2194–2202.
27 M. Calle, H. J. Jo, C. M. Doherty, A. J. Hill and Y. M. Lee, *Macromolecules*, 2015, **48**, 2603–2613.
28 B. Comesaña-Gándara, M. Calle, H. J. Jo, A. Hernández, J. G. de la Campa, J. de Abajo, A. E. Lozano and Y. M. Lee, *J. Memb. Sci.*, 2014, **450**, 369–379.
29 J. L. Santiago-García, C. Álvarez, F. Sánchez and J. G. de la Campa, *J. Memb. Sci.*, 2015, **476**, 442–448.
30 G. L. Tullos, J. M. Powers, S. J. Jeskey and L. J. Mathias, *Macromolecules*, 1999, **32**, 3598–3612.
31 R. Guo, D. F. Sanders, Z. P. Smith, B. D. Freeman, D. R. Paul and J. E. McGrath, *J. Mater. Chem. A*, 2013, **1**, 262–272.
32 J. Kostina, O. Rusakova, G. Bondarenko, A. Alentiev, T. Meleshko, N. Kukarkina, A. Yakimanskii and Y. Yampolskii, *Ind. Eng. Chem. Res.*, 2013, **52**, 10476–10483.
33 E.-S. Yoo, A. J. Gavrin, R. J. Farris and E. B. Coughlin, *High Perform. Polym.*, 2003, **15**, 519–535.
34 S. I. Kim, T. J. Shin, S. M. Pyo, J. M. Moon and M. Ree, *Polymer*, 1999, **40**, 1603–1610.
35 M. Al-Masri, D. Fritsch and H. R. Kricheldorf, *Macromolecules*, 2000, **33**, 7127–7135.
36 M. J. S. Dewar, E. G. Zoebisch, E. F. Healy and J. J. P. Stewart, *J. Am. Chem. Soc.*, 1985, **107**, 3902–3909.
37.
38 A. D. Becke, *J. Chem. Phys.*, 1993, **98**, 5648.
39 C. Lee, W. Yang and R. G. Parr, *Phys. Rev. B*, 1988, **37**, 785–789.
40 W. J. Hehre, L. Radom, P. V. R. Schleyer and J. A. Pople, *Ab Initio Molecular Orbital Theory*, 1986, vol. 9.
41 C. G. and J. A. P. M. J. Frisch, G. W. Trucks, H. B. Schlegel, G. E. Scuseria, M. A. Robb, J. R. Cheeseman, J. A. Montgomery Jr., T. Vreven, K. N. Kudin, J. C. Burant, J.M.Millam, S. S. Iyengar, J. Tomasi, V. Barone, B. Mennucci, M. Cossi, G. Scalmani, N. Rega, G. A. Peters, *Gaussian, Inc., Wallingford CT,* 2004.
42 M. A. Thompson, *Planaria Software LLC, Seattle, WA.*
43 D. M. Muñoz, M. Calle, J. G. de la Campa, J. de Abajo and A. E. Lozano, *Macromolecules*, 2009, **42**, 5892–5894.
44 M. Calle, Y. Chan, H. J. Jo and Y. M. Lee, *Polymer*, 2012, **53**, 2783–2791.
45 B. Comesaña-Gándara, A. Hernández, J. G. de la Campa, J. de Abajo, A. E. Lozano and Y. Moo Lee, *J. Memb. Sci.*, 2015, **493**, 329–339.
46 D. F. Sanders, Z. P. Smith, C. P. Ribeiro, R. Guo, J. E. McGrath, D. R. Paul and B. D. Freeman, *J. Memb. Sci.*, 2012, **409-410**, 232–241.
47 H. B. Park, S. H. Han, C. H. Jung, Y. M. Lee and A. J. Hill, *J. Memb. Sci.*, 2010, **359**, 11–24.
48 S. H. Han, N. Misdan, S. Kim, C. M. Doherty, A. J. Hill and Y. M. Lee, *Macromolecules*, 2010, **43**, 7657–7667.
49 D. F. Sanders, *The effect of synthesis route and ortho-position functional group on thermal rearranged polymer thermal and transport properties*, Ph D dissertation, University of Texas, 2013.
50 J. U. Wieneke and C. Staudt, *Polym. Degrad. Stab.,* 2010, **95**, 684–693.
51 T. Waters, R. A. J. O'Hair and A. G. Wedd, *Int. J. Mass Spectrom.*, 2003, **228**, 599–611.
52 I. V. Farr, D. Kratzner, T. E. Glass, D. Dunson, Q. Ji and J. E. McGrath, *J. Polym. Sci. Part A Polym. Chem.*, 2000, **38**, 2840–2854.
53 W. Xie, R. Heltsley, X. Cai, F. Deng, J. Liu, C. Lee and W.-P. Pan, *J. Appl. Polym. Sci.*, 2002, **83**, 1219–1227.
54 W. Xie, R. Heltsley, H.-X. Li, C. Lee and W.-P. Pan, *J. Appl. Polym. Sci.*, 2002, **83**, 2213–2224.
55 M. Calle and Y. M. Lee, *Macromolecules*, 2011, **44**, 1156–1165.
56 M. Pecullan, K. Brezinsky and I. Glassman, *J. Phys. Chem. A*, 1997, **101**, 3305–3316.
57 G. Tullos and L. Mathias, *Polymer*, 1999, **40**, 3463–3468.

ARTICLE

58 D. Guzmán-Lucero and D. Likhatchev, *Polym. Bull.*, 2002, **48**, 261–269.

59 J. H. Hodgkin, M. S. Liu, B. N. Dao, J. Mardel and A. J. Hill, *Eur. Polym. J.*, 2011, **47**, 394–400.

60 J. H. Hodgkin and B. N. Dao, *Eur. Polym. J.*, 2009, **45**, 3081–3092.

61 C. a. Scholes, C. P. Ribeiro, S. E. Kentish and B. D. Freeman, *J. Memb. Sci.*, 2014, **450**, 72–80.

62 Z. P. Smith, D. F. Sanders, C. P. Ribeiro, R. Guo, B. D. Freeman, D. R. Paul, J. E. McGrath and S. Swinnea, *J. Memb. Sci.*, 2012, **415-416**, 558–567.

63 M. Calle, A. E. Lozano and Y. M. Lee, *Eur. Polym. J.*, 2012, **48**, 1313–1322.

64 Z. P. Smith, G. Hernández, K. L. Gleason, A. Anand, C. M. Doherty, K. Konstas, C. Alvarez, A. J. Hill, A. E. Lozano, D. R. Paul and B. D. Freeman, *J. Memb. Sci.*, 2015, **493**, 766–781.

65 O. Y. Rusakova, Y. V. Kostina, a. S. Rodionov, G. N. Bondarenko, a. Y. Alent'ev, T. K. Meleshko, N. V. Kukarkina and a. V. Yakimanskii, *Polym. Sci. Ser. A*, 2011, **53**, 791–799.

66 S. Li, H. J. Jo, S. H. Han, C. H. Park, S. Kim, P. M. Budd and Y. M. Lee, *J. Memb. Sci.*, 2013, **434**, 137–147.

RSC Advances Accepted Manuscript

208x149mm (300 x 300 DPI)